2019 CMBEC42
Ottawa, ON
May 21-24, 2019
CMBES/SCGB

Infrared Imaging Tools for Necrotizing Enterocolitis (NEC) Diagnosis Guided by RGB-D Sensing

Yangyu Shi[1], Pierre Payeur[1], Monique Frize[2] and Erika Bariciak[3]

[1]School of Electrical Engineering and Computer Science, University of Ottawa, Canada
[2]Department of Systems and Computer Engineering, Carleton University, Canada
[3]Department of Pediatrics, Children's Hospital of Eastern Ontario, Canada

Abstract— **Necrotizing enterocolitis (NEC) is a disease that leads to inflammation in the intestinal tissue of premature babies. In this paper, we present a novel automated image acquisition and processing system that integrates infrared and RGB-D sensors for NEC detection. Inter-sensor calibration and data registration are introduced to ensure the consistency of depth, color and infrared images captured by the multispectral sensor. Segmentation of a baby's torso area is automatically achieved over the infrared imagery while relying on depth and color data to entirely retrieve the region of interest. Analysis of thermal distribution over the whole area reduces the risk of missing key information due to manual intervention. Preliminary results obtained with this multispectral imaging approach for NEC diagnosis are encouraging.**

Keywords— **infrared imaging, NEC diagnosis, RGB-D sensing, image segmentation, thermal distribution analysis.**

I. Introduction

Necrotizing enterocolitis (NEC) affects the gastrointestinal tract of infants. It generates inflammation in intestinal tissue, eventually leading to necrosis, perforation, sepsis and even death. However, the signs of NEC at an early stage are subtle and difficult to detect with current x-ray and ultrasound imaging, but could be monitored via infrared (IR) thermal imaging technology, which measures the thermal field emitted by a body. Given that the normal human body has a normal heat distribution, while an abnormal body state tends to radiate a modified heat distribution, the similarities and differences between the two can assist in clinical diagnosis to infer the nature and extent of a disease [1].

Knobel et al. [2] and Rice et al. [3] determined the differences between normal infants and those diagnosed with NEC by comparing the temperature distribution of the infant's abdominal segments and chest. More recently, Herry et al. [4], Ntonfo et al. [5], and Frize et al. [6] demonstrated the validity of applying infrared thermal imaging to NEC detection in newborns. By analyzing and comparing abdominal thermograms of neonates with confirmed NEC and healthy control newborns, they obtained positive results in distinguishing between NEC infants and infants without NEC.

Although promising results were obtained in previous studies, the operation of the infrared sensor and interpretation of data had limitations. The clinical staff had to manually select areas of interest prior to analysis. Moreover, thermogram analysis was performed only by individuals with specific experience in IR imaging, which was not optimal for a clinical environment. This led to non-uniform acquisition of thermograms, resulting in potential erroneous interpretation. Therefore, with the goal to provide health practitioners with more accurate and easy-to-operate sensing technology for early-stage NEC diagnosis, our goal is to design an automated multispectral imaging approach that combines a thermal IR camera and a RGB-D sensor. The sensors work together during acquisition, and thermogram image processing is automated for streamlined operation and to minimize interference from manual intervention.

II. Methodology

In this study, a Microsoft Kinect Xbox ONE sensor is bundled and calibrated with a FLIR Thermovision A320M thermal infrared camera to simultaneously capture registered images of a baby's body. The IR images record the temperature distribution over the body while the Kinect sensor simultaneously acquires color and depth images (RGB-D). The latter are used in conjunction with the IR images to segment the subject from the background and to remove any visible apparatus, such as probes, tubes and wires, which may lie over the body and may compromise part of the data about temperature distribution. Moreover, the combined inputs make segmentation of the region of interest over the torso of the infant more robust without requiring manual intervention in the image processing stage.

Fig. 1 shows the flow chart of this automated multispectral image acquisition and analysis system. It consists of three main parts: acquisition system design and calibration, automated image segmentation and extraction of

region of interest over the infant`s torso, and temperature distribution analysis. RGB, depth and IR images are registered and adjusted to form a set of images of corresponding resolution, as perceived from the same viewing angle. Background removal, torso segmentation and extraction of the abdominal region are performed based on the characteristics of each image. Finally, pixel values corresponding to temperature data are processed into a thermal signature and statistical measures are applied to analyze variations between NEC and normal infants.

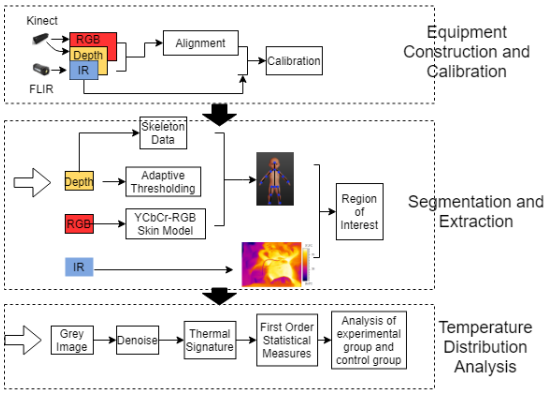

Fig. 1. Multispectral image acquisition and IR data analysis flow chart.

A. Image Acquisition

A Kinect XBox One sensor, shown in Fig. 2a, forms the RGB-D sensor. The embedded RGB camera collects 1920 x 1080 color images; and the depth sensor estimates the relative distance in a map of 512 x 424 pixels. A FLIR A320 infrared camera, shown in Fig. 2b, provides thermal images with a resolution of 320 x 240 pixels.

Since the RGB-D sensor has a wider field of view than the IR camera, it must be positioned closer to the subject than the IR camera. A separation of 20 cm was empirically found to be suitable. In order to ensure that the devices do not occlude each other, the Kinect is also assembled slightly lower than the IR camera, with a vertical separation of 12 cm. Fig. 2c illustrates the configuration of sensors. Since the spectral ranges are respectively 827-850nm for the Kinect depth sensor, and 7.5-13µm for the IR camera, there is no interference between the devices.

(a) (b) (c)

Fig. 2. Imaging devices and their assembly: a) Kinect Xbox One color and depth sensors, b) FLIR A320 infrared camera, and c) assembly of multispectral sensor for a subject located on the right side.

B. Calibration Process

Since the resolution and field of view of the two sensors in the Kinect are not the same, their images cannot be directly matched. Therefore, the first step of calibration is to register the internal devices in the Kinect sensor, to combine depth and color data. Registration is performed in between the color and depth image streams by acquiring images with OpenNI2 registration mode. Depth point coordinates are verified for validity and the corresponding color pixel value is assigned to a matrix with the same size as the depth image. Thus, the alignment produces an image with the appearance of a broken color map, which forms the RGB-D image. Displayed pixels indicate locations where alignment is successful, while black pixels indicate the locations of alignment failure in between the color and depth fields, as shown in Fig. 3.

(a) (b) (c)

Fig. 3. RGB-D images registration: (a) 1920 x 1080 color image, (b) 512 x 424 depth image, (c) 512 x 424 RGB-D image after registration.

Concurrently, the classical checkerboard calibration method is applied for calibration of the Kinect sensor with the IR camera. A customized calibration target was designed for this purpose that embeds LED lights at 50% of the corner locations of a traditional black-and-white checkerboard pattern to support the simultaneous detection of feature points by the color and IR cameras. Therefore, it permits feature points to be matched in between the color and IR images, which facilitates registration in between the sensors. The algorithm used to detect and process the IR feature points is similar to that introduced by Twelves et al. [7]. Multiple checkerboard images are collected from different viewing angles by the Kinect and IR sensors. The GML Calibration Toolbox [8] is used to calculate the intrinsic parameters of the cameras and the extrinsic parameters in between the pairs of images.

C. Segmentation

Since the infrared image contains only temperature information, and the difference in body temperature of each part of the human body is subtle, it is difficult to extract the corresponding abdominal region only by analyzing the IR image. Therefore, we first rely on the depth and color data to segment the infant's torso. The segmentation process is initially driven by the depth. The body is isolated from the background (isolette bedding surface) by applying a distance threshold, as the newborn is typically closer to the sensor, which is installed over the subject

and pointing vertically. As shown in Fig. 4, color information also helps to fine-tune the contours of the body area and to prevent interference from any visible objects. Color coding in the YCbCr space [9, 10] is known to better support the skin color retrieval process because different skin colors are distributed over a small range in the YCbCr space, and only the brightness value, Y, tends to significantly change with the external environment. Since the ambient light in a hospital does not change much when the images of the baby are collected, YCbCr better limits the distribution of skin color, which makes the acquisition system less sensitive to the environment and to various ethnic groups' skin color.

(a) (b) (c)

Fig. 4. Background removal and fine-tuning of the human body contour: (a) original depth image; (b) after removing background based on depth threshold; (c) after applying skin color detector.

Knowledge of the human anatomy provides rich information for finely segmenting the human body from a scene. Moreover, the depth sensor can support an estimation of skeleton data, which refers to the coordinates of a set of joint points that connect parts of the body. Detecting and properly selecting the relevant joint points facilitates the extraction of the region of interest. Hesse et al. [11] proposed a pixelated body part classifier using random ferns. This approach inspired the method proposed here. We first created 15 virtual 3D baby models, as shown in Fig. 5a, using the MakeHuman modeling software [12], and then augmented the data set to 120 by rotating, mirroring, etc. For each model, we selected the effective joint points after fine tuning according to Hesse's work [11]. Here, the joint points do not have to be consistent with anatomically articulated joints. They are only used as critical points to segment different regions. We select 15 joints for each model (Fig. 5b) and extract the depth information from the virtual 3D models. Then for each pixel, we compare the depth of the current pixel with that of pixels in the neighborhood. If the difference in the depth value is smaller than a set threshold, the pixels are associated to a same surface. Then according to the Random Ferns method [11], pixel points are divided into several clusters and each cluster is associated with a joint probability. We use the naïve Bayes classification method to generate the classifier in combination with the preset joint information, the label of each class, and the joint probability. By using the classifier, we can divide the body into different areas based on the depth data, and extract the abdominal area, as shown in yellow in Fig. 5(c), which is our region of interest for NEC diagnosis.

(a) (b) (c)

Fig. 5. Mock-up models: (a) an infant model created by MakeHuman software [12], (b) 15 joint points selected according to experimental needs, (c) abdominal area extracted by the classifier.

D. Temperature Distribution Analysis

After successful extraction of the region of interest, we directly analyze the temperature over the entire region. We first convert the IR image into a grayscale image that represents the temperature distribution over the abdominal area. First order statistics (mean, median, variance, standard deviation, interquartile range, etc) are used to compare between NEC and normal infants, as in previous work [5]. It is effective to use the data differences to describe and distinguish between two groups because babies in the NICU rarely can mount a fever under normal circumstances. Even if they do, it is usually due to significant illness such as sepsis, in which case they would be excluded from our study.

III. Results and Discussion

In the earlier study performed by our group, a dataset of infrared IR images was collected by imaging the abdomen of 10 NEC and 19 normal infants. We used this data to validate the proposed segmentation and thermal distribution analysis processes. In [5], only a manually selected rectangular area over the abdomen was used for statistical analysis. We applied the same temperature distribution analysis method for the more extensive abdominal area that is extracted on the same dataset but with the automated segmentation methodology described in Section II. Resulting statistics are reported in Table 1 and Fig. 6, in comparison with results obtained in the previous study [5].

From both sets of experiments, it is clear that the mean and median temperature values are lower on NEC infants than on those who are normal, indicating that abdominal temperature of NEC newborns can be affected by necrosis of the small intestine and poor blood circulation. In the boxplots shown in Fig. 6, we also observe that fewer outliers (blue dots) occur with the new method. In Fig. 6a, the outliers are more numerous and concentrated in the lower temperature range, indicating that the data freedom of both the NEC and the normal group is small, and the data as a whole are left skewed. In the results obtained

with the proposed method, Fig. 6b, only the NEC population exhibits some outliers. Since these are concentrated in the higher temperature range, it can be concluded that the overall abdominal temperature distribution of the NEC infants is right-biased, while the normal infants form a normal distribution.

Table 1. Statistical measures over 10 NEC and 19 normal infants.

	NEC (baseline [5])	Normal (baseline [5])	NEC (proposed)	Normal (proposed)
Mean	185.7	217.87	183.9	222.9
Standard variance	12.2	9.9	16.7	14.9
Median	188	219	184	225
Min	139	154	130	126
Max	217	255	249	255
Skewness	-0.39	-0.78	0.039	-0.99
Median absolute deviation	9.97	7.56	13.31	11.86
Interquartile range	17	20	23	20
Kurtosis	2.7	4.2	3.2	3.6
Sum	1093336	2514164	2260374	5147958

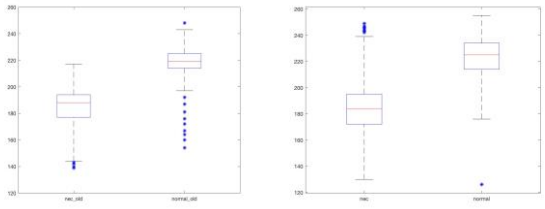

Fig. 6. Boxplots of NEC and normals (left: baseline [5], right: proposed).

IV. Conclusion

In this study, we present a custom multispectral vision sensor, which aims to automate the imaging analysis process for the detection of NEC in newborn infants, making it easier for healthcare professionals to capture and analyze IR images while minimizing the introduction of bias from manual manipulation of data. A procedure for calibration of IR, depth, and color images collected from different viewing positions and resolutions is developed to support the integration of a RGB-D sensor with an IR camera. Depth and color space information is fully leveraged to make up for the shortcomings of traditional segmentation approaches when applied on IR images. The proposed acquisition system and automated segmentation approach lead to a more comprehensive temperature distribution analysis over the entire abdominal region than when manual segmentation was performed over IR images only. Beyond facilitating the work of medical personnel, this can reduce the risk of missing key information. Future work will involve validation and application of this system in a clinical environment with the acquisition of new datasets to further test the approach.

Acknowledgment

The authors acknowledge support from Natural Sciences and Engineering Research Council of Canada.

Conflict of Interest

The authors declare no conflict of interest.

References

1. Lawson, R.N. Thermography - a new tool in the investigation of breast lesions. Can. Serv. Med. J. 1957;13: 517–524.
2. Knobel, R.B, Guenther, B.D., Rice, H.E. "Thermoregulation and thermography in neonatal physiology and disease". Biological research for nursing, 13.3 (2011): 274-282.
3. Rice, H.E., et al. "Infrared thermal imaging (thermography) of the abdomen in extremely low birthweight infants". J. Surg. Radiol. 1.2 (2010): 61-122.
4. Herry, C., Frize, M. Bariciak, E. "Assessment of Abdominal Temperature Change in NEC and Healthy Premature Newborns". Proc. of the Engineering in Medicine and Biology Society Conference (EMBC 2011), 5th European Conference of the International Federation for Medical and Biological Engineering (IFMBE), Vol. 37, 2012, pp 191-194.
5. Ntonfo, G., Frize, M., Bariciak, E. "Detection of Necrotizing Enterocolitis in Newborns using Abdominal Thermal Signature Analysis". IEEE Intl Symp. on Medical Measurements and Applications (MeMeA), Torino, Italy, May 7-9, 2015.
6. Frize, M., Nur, R., Bariciak, E., Herry, C. "Infrared Imaging and Classification of Neonates with Necrotising Enterocolitis". World Congress on Medical Physics and Biomedical Engineering, IFMBE Proceedings, Vol. 39, 2013, pp 1309-1312.
7. Twelves, S., Payeur, P., Frize, M. "Toward the Detection of Overlapping Body Parts in Medical Infrared Images". Proc. of the 34th Canadian Medical and Biological Engineering Society Conference (CMBEC 2011), Toronto, ON, 5-8 Jun. 2011.
8. Graphics and Media Lab, GML C++ Camera Calibration Toolbox, http://graphics.cs.msu.ru/en/node/909.
9. Phung, S. L., Bouzerdoum, A., Chai, D. "A Novel Skin Color Model in YCbCr Color Space and its Application to Human Face Detection". Proc. of IEEE Intl Conf. on Image Processing, Vol. 1, 2002, pp. I289-I292.
10. Bari, C., Ghorude, T.N. "Face Recognition Using Skin Colour Segmentation of YCbCr and RGB Color Models". Intl Journal of Emerging Technology in Computer Science & Electronics (IJERCSE), 23(1), 2016, pp. 976-1353
11. Hesse, N., Stachowiak, G., Breuer, T., Arens, M. "Estimating Body Pose of Infants in Depth Images Using Random Ferns". Proc. of the IEEE Intl Conf. on Computer Vision Workshops, 2015, pp. 35-43.
12. MakeHuman, Open source tool for making 3d characters, www.makehumans.org, Sep. 2015.